AN ANALYTICAL WALL-FUNCTION FOR TURBULENT ROUGH WALL HEAT TRANSFER

K. Suga
Computational Physics Lab.,
Toyota Central Research and Development Laboratories, Inc.
Nagakute, Aichi, 480-1192, Japan
k-suga@mosk.tytlabs.co.jp

T.J. Craft and H. Iacovides
School of Mechanical, Aerospace and Civil Engineering,
The University of Manchester
P.O. Box 88, Manchester, M60 1QD, U.K.
tim.craft@manchester.ac.uk, h.iacovides@manchester.ac.uk

ABSTRACT

This paper reports the development of a refined wall-function strategy for the modelling of turbulent forced convection heat transfer over smooth and rough surfaces. In order to include the effects of fine-grain surface roughness, the present study extends a more fundamental work on the development of advanced wall functions of general applicability. The presently proposed model is validated through comparisons with data available for internal flows through channels and for external flows over flat and curved plates with both smooth and rough surfaces. The validation results suggest that the presently proposed form can be successfully applied to a wide range of heat transfer problems over smooth and fine-grain rough surfaces.

INTRODUCTION

Although many recent low-Reynolds-number (LRN) turbulence models perform satisfactorily, industrial engineers still routinely make use of classical wall-function approaches for representing near-wall turbulence and heat transfer. One reason for this is that, despite advances in computing power, their near-wall resolution requirements make LRN models prohibitively expensive in complex three-dimensional industrial heat and fluid flows. This is particularly true for flows over rough surfaces, which are common in industrial applications. Since one cannot hope to resolve the details of small wall-roughness elements, the wall-function approach is the only practical strategy for such industrial applications.

Despite the above comments, in contrast to many other modelling issues, wall-functions have received little attention over the last few decades. Consequently, the strategies in use have, for the most part, been those proposed in the 1970's that assume semi-logarithmic variations of the near-wall velocity and temperature, and either a constant, or at most a linearly varying, total shear stress between the wall and the near-wall node (e.g. Launder and Spalding, 1974). However, it is well known that such conditions do not apply in flows with strong pressure gradients and separation. Moreover, since a universal scale for turbulent buoyant thermal boundary layers has not been established yet, it is difficult to use empirical wall-functions for such phenomena (Hanjalić, 2002).

For rough wall turbulence, there have been several attempts to replace the wall-function approach, e.g. Aupoix and Spalart (2003), etc. Although these extensions overcome some of the defects of the classical wall-function, they still require a fine grid resolution near the walls. Moreover, there are very few references to alternative approaches for computing rough wall heat transfer in the literature.

In order to address industrial requirements, the UMIST group recently proposed an alternative wall-function strategy for flow over smooth walls which, while still semi-empirical in nature, makes assumptions at a deeper, more general level than the log-law based schemes. The approach is called the analytical wall-function (AWF) and integrates simplified mean flow and energy equations analytically over the control volumes adjacent to the wall, assuming a near-wall variation of the turbulent viscosity (Craft *et al.*, 2002). The resulting analytical expresions then produce the value of the wall shear stress and other quantities which are required over the near wall cell. Following this strategy, the present authors extended the AWF to include the effects of fine-grain surface roughness on the flow field, and successfully validated the approach in several rough-wall turbulent flows involving separation and reattachment (Suga *et al.*, 2005).

This subsequent study focuses on extending and validating the AWF for forced convection rough wall heat transfer. The presently proposed model is validated through comparisons with data available for internal flows through channels and for external flows over flat and curved plates with both smooth and rough surfaces.

WALL-FUNCTION APPROACH

Although the wall-function approach is well known, it may be useful to recall the main features of its implementation.

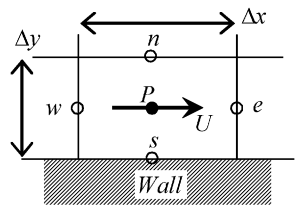

Figure 1: Near-wall grid arrangement.

A simplified transport equation for ϕ near walls:

$$\frac{\partial}{\partial x}(\rho U\phi) = \frac{\partial}{\partial y}\left(\Gamma\frac{\partial\phi}{\partial y}\right) + S_\phi \tag{1}$$

can be integrated using the finite volume method over the cells illustrated in Fig.1 giving

$$\begin{aligned}&\int_s^n\int_w^e \tfrac{\partial}{\partial x}(\rho U\phi)dx\ dy\\ &= \int_s^n\int_w^e \tfrac{\partial}{\partial y}\left(\Gamma\tfrac{\partial\phi}{\partial y}\right)dx\ dy + \int_s^n\int_w^e S_\phi dx\ dy,\end{aligned} \tag{2}$$

$$\begin{aligned}&[(\rho U\phi)_e - (\rho U\phi)_w]\Delta y\\ &= \left[\left(\Gamma\tfrac{d\phi}{dy}\right)_n - \left(\Gamma\tfrac{d\phi}{dy}\right)_s\right]\Delta x + \bar{S}_\phi\Delta x\Delta y\end{aligned} \tag{3}$$

where $\overline{S_\phi}$ is the averaged source term over the cell P. Note that x is the wall parallel coordinate while y is the wall normal coordinate. (Although two-dimensional forms are written here, extending them to three-dimensions is straightforward.)

When the wall parallel component of the momentum equation is considered ($\phi = U$) the term $(\Gamma d\phi/dy)_s$ in Eq.(3) corresponds to the wall shear stress $\tau_w(\equiv \mu\partial U/\partial y|_w)$, while in the energy equation it corresponds to the wall heat flux q_w. Instead of calculating these from the standard discretization, they are obtained from the algebraic wall-function expressions.

In the case of the transport equation for the turbulence energy k in incompressible flows, the averaged source term over the wall adjacent cell is written as

$$\overline{S_k} = \overline{\rho P_k - \rho\varepsilon} = \rho(\overline{P_k} - \overline{\varepsilon}). \tag{4}$$

The terms $\overline{P_k}$ and $\overline{\varepsilon}$ thus also need to be provided by the wall-function.

AWF for smooth wall heat transfer

Before discussing the extension for rough wall heat transfer, it is useful to summarise the standard AWF by Craft *et al.*(2002).

In the AWF, the wall shear stress and heat flux are obtained through the analytical solution of simplified near-wall versions of the transport equation for the wall-parallel momentum and temperature. The main assumption required for the analytical integration of the transport equations is a prescribed variation of the turbulent viscosity μ_t, expressed using $y_v^*(\equiv y_v k_P^{1/2}/\nu)$ as the thickness of viscosity dominated sub-layer as

$$\mu_t = \max\left\{0, \alpha\mu\left(y^* - y_v^*\right)\right\}. \tag{5}$$

In the context of Fig.2, the near-wall simplified forms of the momentum and energy equations become

$$\frac{\partial}{\partial y^*}\left[\left(\mu + \mu_t\right)\frac{\partial U}{\partial y^*}\right] = \underbrace{\frac{\nu^2}{k_P}\left[\frac{\partial}{\partial x}\left(\rho UU\right) + \frac{\partial P}{\partial x}\right]}_{C_U} \tag{6}$$

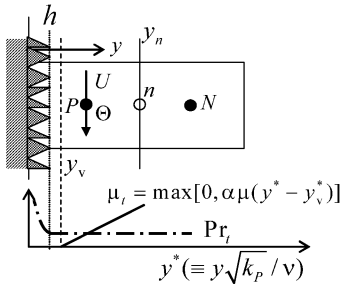

Figure 2: Near-wall cells.

Table 1: Model coefficients.

α	c_ℓ	c_μ	y_{vs}^*	y_ε^*	Pr_t^∞
$c_\ell c_\mu$	2.55	0.09	10.7	5.1	0.9

$$\frac{\partial}{\partial y^*}\left[\left(\frac{\mu}{Pr} + \frac{\mu_t}{Pr_t}\right)\frac{\partial\Theta}{\partial y^*}\right] = \underbrace{\frac{\nu^2}{k_P}\left[\frac{\partial}{\partial x}\left(\rho U\Theta\right) + S_\theta\right]}_{C_T} \tag{7}$$

where Pr_t is a prescribed turbulent Prandtl number, taken as 0.9. Further assumptions are that convective transport and the wall-parallel pressure gradient $\partial P/\partial x$ do not change across the wall-adjacent cell. Thus, the right hand side terms C_U and C_T of Eqs.(6) and (7) can be treated as constant. Then, the equations can be integrated analytically over the wall-adjacent cell giving

$$\frac{dU}{dy^*} = \begin{cases} (C_U y^* + A_U)/\mu, \text{ if } y^* < y_v^* \\ \frac{C_U y^* + A_U'}{\mu\{1+\alpha(y^* - y_v^*)\}}, \text{ if } y^* \geq y_v^* \end{cases} \tag{8}$$

$$\frac{d\Theta}{dy^*} = \begin{cases} Pr(C_T y^* + A_T)/\mu, \text{ if } y^* < y_v^* \\ \frac{Pr(C_T y^* + A_T')}{\mu\{1+\alpha Pr(y^* - y_v^*)/Pr_t\}}, \text{ if } y^* \geq y_v^*. \end{cases} \tag{9}$$

Further integration to obtain U and Θ is also straightforward. The integration constants A_U, A_T etc. are determined by applying boundary conditions at the wall, at y_v and the point n. The values at n are determined by interpolation between the calculated node values at P and N, whilst at y_v a monotonic distribution condition is imposed by ensuring that U, Θ and their gradients should be continuous at $y = y_v$.

The result is that the wall shear stress and wall heat flux can be expressed as

$$\tau_w = \mu\left.\frac{dU}{dy}\right|_w = \mu\frac{k_P^{1/2}}{\nu}\left.\frac{dU}{dy^*}\right|_w = \frac{k_P^{1/2}A_U}{\nu} \tag{10}$$

$$q_w = -\frac{\rho c_p\nu}{Pr}\left.\frac{d\Theta}{dy}\right|_w = -\frac{\rho c_p\nu}{Pr}\frac{k_P^{1/2}}{\nu}\left.\frac{d\Theta}{dy^*}\right|_w = -\frac{\rho c_p k_P^{1/2}A_T}{\mu}. \tag{11}$$

The local generation rate of k, $P_k(=\nu_t(\frac{dU}{dy})^2)$, is written as

$$P_k = \begin{cases} 0, \text{ if } y^* < y_v^* \\ \frac{\alpha k_P}{\nu}(y^* - y_v^*)\left(\frac{C_U y^* + A_U'}{\mu\{1+\alpha(y^* - y_v^*)\}}\right)^2, \text{if } y^* \geq y_v^* \end{cases} \tag{12}$$

which can then be integrated over the wall-adjacent cell to produce an average value $\overline{P_k}$ for use in solving the k equation.

For the dissipation rate ε, the following model is employed:

$$\varepsilon = \begin{cases} 2\nu k_P/y_\varepsilon^2, \text{ if } y < y_\varepsilon \\ k_P^{1.5}/(c_\ell y), \text{ if } y \geq y_\varepsilon. \end{cases} \tag{13}$$

The characteristic dissipation scale y_ε can be defined as $y_\varepsilon^* = 2c_\ell$ to ensure a continuous variation of ε at y_ε. Thus, the cell averaged value is obtained as

$$\overline{\varepsilon} = \begin{cases} 2k_P^2/(\nu y_\varepsilon^{*2}), \text{ if } y_\varepsilon^* > y_n^* \\ \frac{1}{y_n}(y_\varepsilon\frac{2\nu k_P}{y_\varepsilon^2} + \int_{y_\varepsilon}^{y_n}\frac{k_P^{1.5}}{c_\ell y}dy) \\ = \frac{k_P^2}{\nu y_n^*}\left[\frac{2}{y_\varepsilon^*} + \frac{1}{c_\ell}\ln\left(\frac{y_n^*}{y_\varepsilon^*}\right)\right], \text{ if } y_\varepsilon^* \leq y_n^*. \end{cases} \tag{14}$$

The value of the constant y_v^* was optimized to be 10.7 through numerical experiments. The other model coefficients are listed in Table 1.

Table 2: Cell averaged generation:$\overline{P_k}$, and integration constant: A_U.

case	$\overline{P_k}$
(a) $y_v < 0$	$\frac{\alpha}{\mu^2 y_n^*}\frac{k_P}{\nu}\left\{\int_0^{h^*}(y^*-y_v^*)\left(\frac{A_U}{Y^*}\right)^2 dy^* + \int_{h^*}^{y_n^*}(y^*-y_v^*)\left(\frac{C_U(y^*-h^*)+A_U}{Y^*}\right)^2 dy^*\right\}$
(b) $0 \le y_v \le h$	$\frac{\alpha}{\mu^2 y_n^*}\frac{k_P}{\nu}\left\{\int_{y_v^*}^{h^*}(y^*-y_v^*)\left(\frac{A_U}{Y^*}\right)^2 dy^* + \int_{h^*}^{y_n^*}(y^*-y_v^*)\left(\frac{C_U(y^*-h^*)+A_U}{Y^*}\right)^2 dy^*\right\}$
(c) $h \le y_v \le y_n$	$\frac{\alpha}{\mu^2 y_n^*}\frac{k_P}{\nu}\int_{y_v^*}^{y_n^*}(y^*-y_v^*)\left(\frac{C_U(y^*-h^*)+A_U}{Y^*}\right)^2 dy^*$
(d) $y_n \le y_v$	0
case	A_U
(a) $y_v < 0$	$\left\{\alpha\mu U_n - C_U(y_n^*-h^*) + C_U(\frac{Y_0^*}{\alpha}+h^*)\ln[Y_n^*/Y_h^*]\right\}\Big/\ln[Y_n^*/Y_0^*]$
(b) $0 \le y_v \le h$	$\left\{\alpha\mu U_n - C_U(y_n^*-h^*) + C_U(\frac{Y_0^*}{\alpha}+h^*)\ln[Y_n^*/Y_h^*]\right\}\Big/(\alpha y_v^* + \ln Y_n^*)$
(c) $h \le y_v \le y_n$	$\left\{\alpha\mu U_n - C_U(y_n^*-y_v^*) + C_U(\frac{Y_0^*}{\alpha}+h^*)\ln Y_n^* - \frac{\alpha}{2}C_U(y_v^{*2}-2h^*y_v^*+h^{*2})\right\}\Big/(\alpha y_v^* + \ln Y_n^*)$
(d) $y_n \le y_v$	$\left\{\mu U_n - \frac{1}{2}C_U(y_n^{*2}-2h^*y_n^*+h^{*2})\right\}\Big/y_n^*$

Table 3: Coefficients in Eq.(22).

case	D
(a) $y_v < 0$	$\frac{-\beta_T h^*}{\alpha_T-\beta_T} + \frac{\alpha_T Y_h^{\beta T}}{(\alpha_T-\beta_T)^2}\ln(Y_h^{\alpha T}/\lambda_b) + \frac{1}{\alpha_T}\ln(Y_n^{\alpha T}/Y_h^{\alpha T})$
(b) $0 \le y_v \le h$	$\frac{\alpha_T y_v^* - \beta_T h^*}{\alpha_T-\beta_T} + \frac{\alpha_T Y_h^{\beta T}}{(\alpha_T-\beta_T)^2}\ln(Y_h^{\alpha T}/Y_h^{\beta T}) + \frac{1}{\alpha_T}\ln(Y_n^{\alpha T}/Y_h^{\alpha T})$
(c) $h \le y_v \le y_n$	$\frac{1}{\alpha_T}\ln Y_n^{\alpha T} + y_v^*$
(d) $y_n \le y_v$	y_n^*
case	E
(a) $y_v < 0$	$\frac{h^*-y_n^*}{\alpha_T} + \frac{1}{\alpha_T}\{\frac{Y_0^{\alpha T}}{\alpha_T} + h^* - \frac{Y_h^{\alpha T}}{\alpha_T-\beta_T}(\frac{\lambda_b\beta_T}{\alpha_T-\beta_T}+1) + \frac{\lambda_b\alpha_T Y_h^{\beta T}}{(\alpha_T-\beta_T)^2}\}\ln(Y_n^{\alpha T}/Y_h^{\alpha T})$ $+\frac{\alpha_T\lambda_b Y_h^{\beta T}}{(\alpha_T-\beta_T)^3}\ln(Y_h^{\alpha T}/\lambda_b) - \frac{h^*}{\alpha_T-\beta_T}(1+\frac{\beta_T h^*}{2}+\frac{\beta_T\lambda_b}{\alpha_T-\beta_T})$
(b) $0 \le y_v \le h$	$\frac{h^*-y_n^*}{\alpha_T} + \frac{1}{\alpha_T}\{\frac{Y_0^{\alpha T}}{\alpha_T} + h^* - \frac{Y_h^{\alpha T}}{\alpha_T-\beta_T}(\frac{\lambda_b\beta_T}{\alpha_T-\beta_T}+1) + \frac{\lambda_b\alpha_T Y_h^{\beta T}}{(\alpha_T-\beta_T)^2}\}\ln(Y_n^{\alpha T}/Y_h^{\alpha T})$ $+\frac{\alpha_T\lambda_b Y_h^{\beta T}}{(\alpha_T-\beta_T)^3}\ln(Y_h^{\alpha T}/Y_h^{\beta T}) - \frac{h^*}{\alpha_T-\beta_T}(1+\frac{\beta_T h^*}{2}+\frac{\beta_T\lambda_b}{\alpha_T-\beta_T}) + \frac{y_v^*}{\alpha_T-\beta_T}(\frac{\alpha_T Y_h^{\beta T}}{\alpha_T-\beta_T} - \frac{\alpha_T y_v^*}{2})$
(c) $h \le y_v \le y_n$	$\frac{y_v^*-y_n^*}{\alpha_T} - y_v^{*2}/2 + \frac{Y_0^{\alpha T}}{\alpha_T^2}\ln Y_n^{\alpha T}$
(d) $y_n \le y_v$	$-y_n^{*2}/2$

Extension for rough wall heat transfer

In common with conventional wall-functions, the extension of the AWF strategy to flows over rough surfaces involves the use of the dimensionless roughness height, h^*. In this case, however, h^* is used to modify the near-wall variation of the turbulent viscosity. More specifically, y_v^* is no longer fixed at 10.7, but instead it becomes a function of h^* as

$$y_v^* = y_{vs}^*\{1-(h^*/70)^m\} \tag{15}$$

$$m = \max\left\{\left(0.5 - 0.4\left(\frac{h^*}{70}\right)^{0.7}\right), \left(1 - 0.79\left(\frac{h^*}{70}\right)^{-0.28}\right)\right\} \tag{16}$$

The function for the index, m, has been determined through a series of numerical experiments and comparisons with available data. For $y_v^* > 0$, corresponding to transitional roughness with $h^* < 70$, the analytical solutions derived for smooth walls can still be used, but with the above modified value for y_v^*. When $y_v^* < 0$, corresponding to a fully-rough surface with $h^* > 70$, the viscosity-dominated sub-layer is destroyed.

Unlike in a sublayer over a smooth wall, the total shear stress now includes the drag force from the roughness elements in the inner layer which is proportional to the local velocity squared and becomes dominant away from the wall, compared to the viscous force. This implies that the convective and pressure gradient contributions should be represented somewhat differently across the inner layer, below the roughness element height. Hence, the practice of simply evaluating the rhs of Eq.(6) in terms of nodal values needs modifying. In the present study a simple approach has been taken, by assuming that the total shear stress remains constant across the roughness element height. Consequently, one is led to

$$C_U = \begin{cases} 0, \text{ if } y^* \le h^* \\ \frac{\nu^2}{k_P}\left[\frac{\partial}{\partial x}(\rho UU) + \frac{\partial P}{\partial x}\right], \text{ if } y^* > h^*. \end{cases} \tag{17}$$

In the energy equation, Pr_t is also no longer constant over the wall-adjacent cell. The reason for this is that, since the fluid trapped behind a roughness element forms a thermal barrier, the turbulent transport of the thermal energy is effectively reduced relative to the momentum transport. (The results of rib-roughened channel flow DNS by Nagano *et al.*(2004) support this consideration since the obtained turbulent Prandtl number increases significantly toward the wall between the riblets.) Thus, after a series of numerical ex-

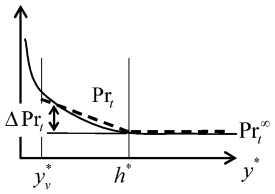

Figure 3: Modelled turbulent Prandtl number distribution.

periments, the following form has been adopted within the roughness elements ($y \le h$).

$$Pr_t = Pr_t^{\infty} + \Delta Pr_t \tag{18}$$

$$\Delta Pr_t = C_0 \max(0, 1 - y^*/h^*) \tag{19}$$

$$C_0 = \frac{5.5}{1 + (h^*/70)^{6.5}} + 0.6 \tag{20}$$

Although it might be better to model the distribution of Pr_t with a non-linear function, a simple linear profile (Eq.(19)) is assumed in the roughness region of $y \le h$ as illustrated in Fig.3. Note that since the turbulent viscosity is defined as zero in the region $y < y_v$, the precise profile adopted for the turbulent Prandtl number in the viscous sub-layer ($y < y_v$) does not affect the computation. Over the rest of the field ($y > h$), $Pr_t = Pr_t^{\infty}$ is applied.

The analytical solutions of both mean flow and energy equations then can be obtained in the four different cases illustrated in Fig.4. Note that it is assumed that the wall-adjacent cell height is always greater than the roughness height. Even in the case without any viscous sub-layer (case(a)), the resultant expressions for τ_w and q_w are of the same form as those of Eqs.(10) and (11). However, different values of A_U and A_T are obtained, corresponding to the four different cases.

In Table 2, the cell averaged generation term $\overline{P_k}$ and A_U are listed, introducing $Y^* \equiv 1+\alpha(y^*-y_v^*)$. Note that Eqs.(13) and (14) are still used for the dissipation, and the integration for $\overline{P_k}$ in Table 2 can be performed as follows.

$$\int (y - y_v) \left(\frac{Cy + A}{1 + \alpha(y - y_v)} \right)^2 dy$$

$$= \frac{C^2}{2\alpha^2} y^2 + \frac{C(2A + Cy_v - 2C/\alpha)}{\alpha^2} y + \frac{(A + Cy_v - C/\alpha)^2}{\alpha^2 [1 + \alpha(y - y_v)]}$$

$$+ \frac{(A + Cy_v - C/\alpha)(A + Cy_v - 3C/\alpha)}{\alpha^2} \ln[1 + \alpha(y - y_v)]$$

$$+ const. \tag{21}$$

For heat transfer, the resultant form of the integration constant A_T can be written as

$$A_T = \{\mu(\Theta_n - \Theta_w)/Pr + C_T E\}/D \tag{22}$$

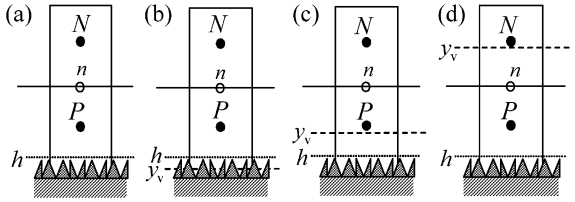

Figure 4: Near-wall cells over a rough wall.

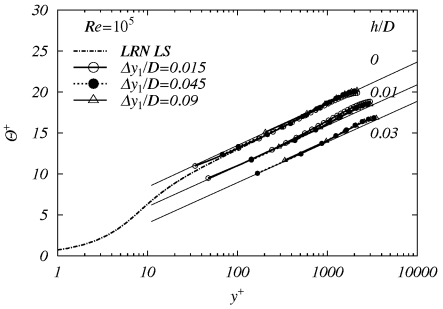

Figure 5: Mean temperature in channel flows at $Pr = 0.71$; lines with symbols: AWF+$k-\varepsilon$, solid thin lines: log law profiles.

where the coefficients D and E are listed in Table 3, defining $\alpha_T \equiv \alpha Pr/(Pr_t^{\infty})$, $\beta_T \equiv C_0/(h^* Pr_t^{\infty})$, $Y^{\alpha T} \equiv 1 + \alpha_T(y^* - y_v^*)$, $Y^{\beta T} \equiv 1 + \beta_T(y^* - y_v^*)$, and $\lambda_b \equiv Y_0^{\alpha T} + \beta_T h^*$.

In the case of constant wall heat flux conditions, the wall temperature is obtained by rewriting Eqs.(11) and (22) as

$$\Theta_w = \Theta_n + \frac{Prq_w}{\rho c_p k_P^{1/2}} D + \frac{PrC_T E}{\mu}. \tag{23}$$

RESULTS AND DISCUSSIONS

The CFD code used in this study is a finite-volume code STREAM (Lien and Leschziner, 1994). The code employs the SIMPLE pressure-correction algorithm on a non-orthogonal collocated grid system with the third order MUSCL type scheme for convection terms. The AWF has been implemented with the "standard" linear $k-\varepsilon$ (Launder and Spalding, 1974) and also with a cubic non-linear $k-\varepsilon$ model (Craft *et al.*, 1996: CLS) for the core-region flow turbulence. For the turbulent heat flux in the core-region, the usual eddy diffusivity model with a prescribed turbulent Prandtl number $Pr_t = 0.9$ is used.

Channel flows

Fig.5 shows the mean temperature distribution in turbulent channel flows at $Re = 10^5$ and $Pr = 0.71$ on a variety of computational grids. In the smooth wall case ($h/D = 0$), with any grid spacing, the AWF well reproduces the result of the LRN $k-\varepsilon$ model (Launder and Sharma, 1974: LS) and the log law (Johnk and Hanratty, 1962):

$$\Theta^+ = 3.3 + 2.21 \ln y^+. \tag{24}$$

The meshes used have 49, 19 and 14 nodes across the channel, resulting in wall-adjacent cell heights of $\Delta y_1/D$ =0.015, 0.045, 0.09.

In the cases of rough walls with $h/D = 0.01, 0.03$, it is clear that the AWF well reproduces the log law distribution for rough walls (Kays and Crawford, 1993):

$$\Theta^+ = \frac{1}{0.8 Re_h^{-0.2} Pr^{-0.44}} + \frac{Pr_t}{\kappa} \ln \frac{32.6 y^+}{Re_h} \tag{25}$$

where $Re_h = u_\tau h/\nu$ and $\kappa = 0.42$. Note that in the case of $h/D = 0.03$, the corresponding roughness Reynolds number is $Re_h \simeq 220$ which is well in the fully rough regime, while $h/D = 0.01$ corresponds to $Re_h \simeq 60$ which is still in the

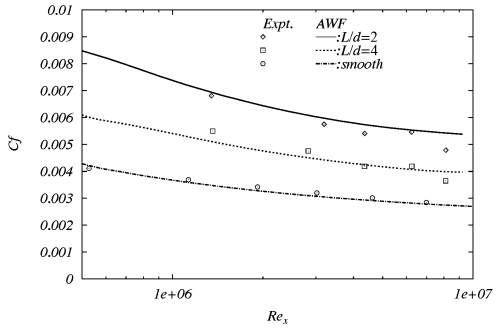

Figure 6: Friction coefficient C_f in rough wall boundary layers.

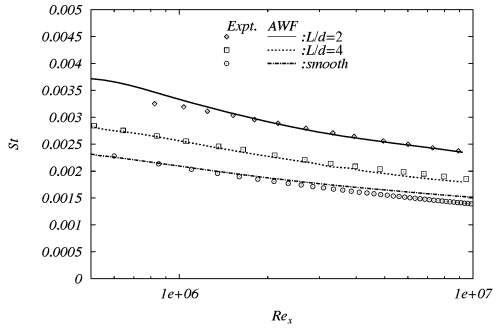

Figure 7: Stanton number distribution in rough wall boundary layers at $Pr = 0.71$.

transitional roughness regime. For each roughness case, profiles from more than one grid are plotted. Since the AWF is quite insensitive to near-wall grid size, discrepancies between the profiles are hardly seen.

Flat plate thermal boundary layers

Hosni *et al.*(1991) measured Stanton number St distribution in zero pressure gradient isothermally heated rough wall boundary layer flows. They arranged hemispherical roughness elements on the base of their wind tunnel. According to Schlichting (1979), their cases of $L/d = 2, 4$ respectively correspond to 0.63, 0.1 mm of the equivalent sand grain roughness heights h. Consequently, the flow regimes correspond to the fully rough ($Re_h \equiv u_\tau h/\nu \simeq 120$) and the transitional roughness regimes ($Re_h \simeq 16$), respectively.

Fig.6 compares the friction factor C_f distribution obtained by the AWF with the standard $k-\varepsilon$ model and the experimental results. It is confirmed that the predicted profiles are reasonable for the rough wall cases as well as the smooth wall case.

Fig.7 shows the comparison in the distribution of St. It can be seen that the present predictions accord well with the experimentally obtained values. For the surface with $L/d = 4$, the increase in St over the smooth wall case is about 40%; and for $L/d = 2$ the increase is about 75%. This increase of St due to the roughness is correctly predicted. Note that the profile of the experimental smooth wall case is from the correlation shown in Hosni *et al.*(1991):

$$St = 0.185(\log_{10} Re_x)^{-2.584} Pr^{-0.4}. \qquad (26)$$

Fig.8 compares the mean temperature distribution at the point of $Re_x = 10^6$. The log law lines are from Eq.(25). Although the predicted profiles are a little lower than the log law profiles, the agreement is satisfactory.

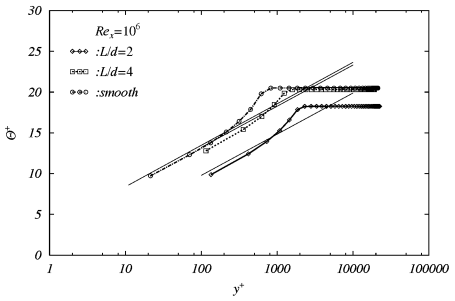

Figure 8: Mean temperature in rough wall boundary layers at $Pr = 0.71$; lines with symbols: AWF+$k-\varepsilon$, solid thin lines: log law profiles.

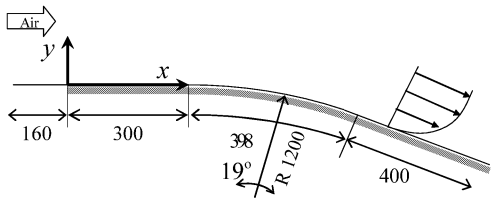

Figure 9: Flow geometry of the convex rough wall boundary layers of Turner *et al.*(2000).

Curved wall thermal boundary layers

Heat transfer along curved surfaces is very common and important in engineering applications such as in heat sinks and around turbine blades. Thus, although the AWF itself does not explicitly include sensitivity to streamline curvature, it is useful to confirm its performance when applied in combination with a turbulence model which does capture streamline curvature effects. Hence, the turbulence model used here is the cubic non-linear $k-\varepsilon$ model (CLS).

For comparison, the rough wall heat transfer experiments over a convex surface by Turner *et al.*(2000) are chosen. The flow geometry is shown in Fig.9. (Since its curved section is so short, it is impossible to discuss fully developed characteristics of the curved flow. However, as far as the present authors are aware, other such fundamental measurements have not been reported in the literature.) The working fluid was air at room temperature and the wall was isothermally heated. The comparison is made in the cases of trapezoidal shaped roughness elements. According to Turner *et al.*, the equivalent sand grain roughness height h is 1.1 times the element height.

Fig.10 compares the Nusselt number Nu distribution under zero pressure gradient conditions. Fig.10(a) shows the case of $h = 0.55mm$. The inlet velocities of $U_0 = 40,\ 22m/s$ respectively correspond to $Re_h \simeq 90, 50$ and thus they are in the full and the transitional roughness regimes. In the case of $h = 0.825mm$, shown in Fig.10(b), $U_0 = 40, 22m/s$ correspond to $Re_h \simeq 135, 80$ which are both in the fully rough regime. From the comparisons, although there can be seen some discrepancy, it is recognised that the agreement between the experiments and the predictions is acceptable in both the full and transitional roughness regimes.

Fig.10 also shows the effects of the wall curvature on the heat transfer coefficients in the case of $U_0 = 40m/s$. (The

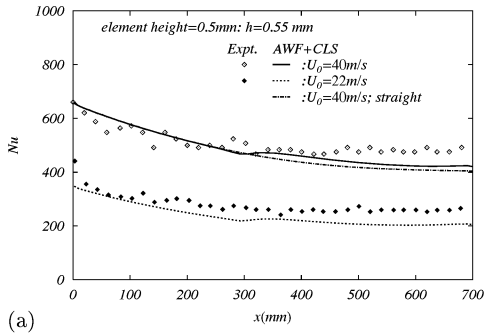

(a)

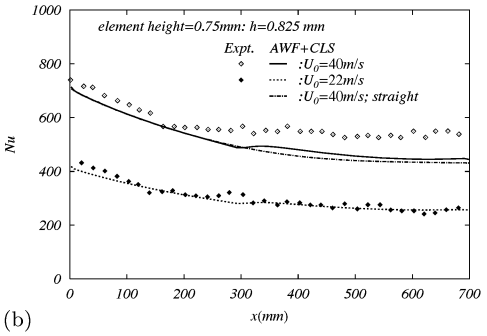

(b)

Figure 10: Nusselt number distribution in convex rough wall boundary layers at Pr=0.71.

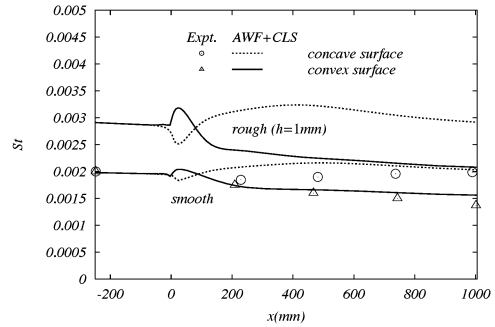

Figure 11: Stanton number distribution in convex and concave wall boundary layers at Pr=0.71.

curved section is in the region of $300mm < x < 698mm$.) Although the curvature effects observed are not large, since the curvature is not very strong, they are certainly predicted by the present computations with the AWF and cubic non-linear $k-\varepsilon$ model. Turner *et al.*(2000) reported that the curvature appeared to cause an increase of 2 to 3% in Nu. Computations are consistent with this experimental observation. However, it is normally recognised that the turbulence along a convex surface tends to be damped as does the heat transfer, unlike in Turner *et al.*'s cases. Thus, additional tests on curved flows are made as follows.

Fig.11 shows the Stanton number distribution in boundary layers over the convex and concave surfaces of Gibson *et al.*(1984). For both the convex and the concave cases, the curved section whose radius is $R = 0.41m$ starts at the point $x = 0mm$. In the smooth wall cases, the computation reasonably predicts the experimental profiles in which the Stanton number is reduced along the convex surface while it increases along the concave surface. In contrast to this general tendency, in the initial region of curvature, the Stanton number increases slightly along the convex surface before it starts to decrease. Consequently, St on the convex surface is greater than that on the concave surface in the region $0 < x < 100mm$. In the case of the concave surface, there can be seen the totally opposite profile of St.

In the rough wall cases with $h = 1mm$, the tendency of St is the same as for the smooth wall, although its magnitude is increased due to the wall roughness. There are no experimental data for rough walls, but the computation clearly suggests that in the initial stage of the convex curvature, the heat transfer increases before starting to decrease as the flow develops, and in the concave case the opposite tendency can be seen. Turner *et al.*'s measurements were in the initial stages of the convex surface curvature, and thus the tendency shown by both the experiments and the present computations does appear consistent.

CONCLUDING REMARKS

An extended version of the AWF for rough wall heat transfer is proposed and validated in fully developed channel, developing flat plate boundary layer and curved boundary layer flows. The concluding remarks from the present study are:

(1) The effect of wall roughness on heat transfer has been modelled by introducing a dependence on equivalent sand grain roughness into the turbulent Prandtl number.

(2) The present AWF model can be applied successfully to rough wall heat transfer and reproduces the log law profiles of rough wall mean temperatures without significant grid dependency.

(3) The combination of the AWF and the cubic non-linear $k-\varepsilon$ model has been shown to predict heat transfer from a curved rough wall with reasonable accuracy.

REFERENCES

Aupoix, B., Spalart, P.R., 2002, *Int. J. Heat Fluid Flow,* Vol. 24, pp.454–462.

Craft, T.J., Gerasimov, A.V., Iacovides, H., Launder, B.E., 2002, *Int. J. Heat Fluid Flow,* Vol. 23, pp.148–160.

Craft, T.J., Launder, B.E., Suga, K., 1996, *Int. J. Heat Fluid Flow,* Vol. 17, pp.108–115.

Gibson M.M., Verriopoulos C.A., 1984, *Expt. Fluids,* Vol. 2, No.2, pp.73–80.

Hanjalić, K., 2002, *Annu. Rev. Fluid Mech.,* Vol. 34, pp.321–47.

Hosni, M.H., Coleman, H.W., Taylor, R.P., 1991, *Int. J. Heat Mass Transfer,* Vol. 34, pp.1067–1082.

Johnk, R.E., and Hanratty, T.J., 1962, *Chem. Engng. Sci.,* Vol. 17, pp.867–879.

Kays, W.M., Crawford, M.E., 1993, in *Convective Heat and Mass Transfer,* 3rd ed., McGraw-Hill, pp.298–301.

Launder, B.E., and Sharma, B.I., 1974, *Lett. Heat Mass Transfer,* Vol. 1, pp.131–138.

Launder, B.E., Spalding, D.B., 1974, *Comp. Meth. Appl. Mech. Engng.,* Vol. 3, pp.269–289.

Lien, F.S., Leschziner, M.A., 1994, *Comp. Meth. Appl. Mech. Engng.,* Vol. 114, pp.123–148.

Nagano,Y., Hattori,H., Houra,T., 2004, *Int. J. Heat Fluid Flow,* Vol. 25, pp.393–403.

Schlichting, H., 1979, in *Boundary-Layer Theory,* 7th ed., McGraw-Hill, pp.515–626, 652–665.

Suga, K., Craft, T.J., Iacovides, H., 2005, in *Proc. ETMM6*, Sardinia, Italy.

Turner, A.B., Hubbe-Walker, S.E., Bayley, F.J., 2000, *Int. J. Heat Mass Transfer,* Vol. 43, pp.251–262.